AGU PUBLICATIONS

JGR

Journal of Geophysical Research: Earth Surface

RESEARCH ARTICLE
10.1002/2016JF004035

Key Points:
- Tidal inlet migration rate depends on alongshore sediment bypassing and flood-tidal delta deposition
- We parameterize Delft3D-SWAN model experiments to predict tidal inlet migration rates
- We compared migration prediction to 57 (22 unaltered) inlets along the U.S. coastline and find good agreement

Supporting Information:
- Supporting Information S1
- Movie S1

Correspondence to:
J. H. Nienhuis,
jnienhui@tulane.edu

Citation:
Nienhuis, J. H., and A. D. Ashton (2016), Mechanics and rates of tidal inlet migration: Modeling and application to natural examples, *J. Geophys. Res. Earth Surf.*, *121*, 2118–2139, doi:10.1002/2016JF004035.

Received 21 JUL 2016
Accepted 21 OCT 2016
Accepted article online 23 OCT 2016
Published online 10 NOV 2016

Mechanics and rates of tidal inlet migration: Modeling and application to natural examples

Jaap H. Nienhuis[1,2,3] and Andrew D. Ashton[1]

[1]Geology and Geophysics, Woods Hole Oceanographic Institution, Woods Hole, Massachusetts, USA, [2]Earth, Atmospheric and Planetary Science, Massachusetts Institute of Technology, Cambridge, Massachusetts, [3]Department of Earth and Environmental Sciences, Tulane University of Louisiana, New Orleans, Louisiana

Abstract Tidal inlets on barrier coasts can migrate alongshore hundreds of meters per year, often presenting great management and engineering challenges. Here we perform model experiments with migrating tidal inlets in Delft3D-SWAN to investigate the mechanics and rates of inlet migration. Model experiments with obliquely approaching waves suggest that tidal inlet migration occurs due to three mechanisms: (1) littoral sediment deposition along the updrift inlet bank, (2) wave-driven sediment transport preferentially eroding the downdrift bank of the inlet, and (3) flood-tide-driven flow preferentially cutting along the downdrift inlet bank because it is less obstructed by flood-tidal delta deposits. To quantify tidal inlet migration, we propose and apply a simple mass balance framework of sediment fluxes around inlets that includes alongshore sediment bypassing and flood-tidal delta deposition. In model experiments, both updrift littoral sediment and the eroded downdrift inlet bank are sediment sources to the growing updrift barrier and the flood-tidal delta, such that tidal inlets can be net sink of up to 150% of the littoral sediment flux. Our mass balance framework demonstrates how, with flood-tidal deltas acting as a littoral sediment sink, migrating tidal inlets can drive erosion of the downdrift barrier beach. Parameterizing model experiments, we propose a predictive model of tidal inlet migration rates based upon the relative momentum flux of the inlet jet and the alongshore radiation stress; we then compare these predicted migration rates to 22 natural tidal inlets along the U.S. East Coast and find good agreement.

1. Introduction

1.1. Objectives

Tidal inlets in barrier island chains are confined channels maintained by tidal currents that convey water and sediment between lagoonal basins and the ocean (Figure 1a). Obliquely approaching waves move sediment along the shore, which affects the morphology of tidal inlets [*Johnson*, 1919] and can cause inlets to migrate alongshore up to hundreds of meters per year (Figure 1b). Inlet migration has long been recognized to shape the morphology of barrier coasts [*Hayes*, 1980; *Moslow and Tye*, 1985] and to affect the long-term landward movement of barrier islands [*Pierce*, 1970; *Leatherman*, 1979]. Therefore, understanding the mechanics and rates of tidal inlet migration is critical for predicting the morphologic evolution of barrier coastlines under modern and future sea level rise and anthropogenic change. More importantly, predictions of inlet migration rates can provide direct solutions to pressing coastal management challenges.

As the processes that lead to inlet migration are poorly understood, we are unaware of any available method to predict the migration rate of tidal inlets. Here we perform numerical experiments using the coupled hydrodynamic and morphodynamic model Delft3D-SWAN [*Deltares*, 2014] to investigate inlet migration mechanisms. We simulate fully developed migrating tidal inlets in idealized barrier island environments, driven by obliquely approaching waves and a normally incident tide. Using these model experiments, we present a predictive model of tidal inlet migration rates which we compare to natural examples.

1.2. Tidal Inlets

Holocene sea level rise and the drowning of low-gradient continental shelves resulted in the widespread formation of modern barrier islands that separate coastal basins from the open ocean [*McGee*, 1890]. Barrier islands are narrow, low-lying strips of land, and susceptible to breaching during storms [*Johnson*, 1919]. Barrier breaches can become more permanent tidal inlets as long as tidal currents are strong enough to transport sediment in the inlet channel [*Escoffier*, 1940]. As such, the tidal discharge through the channel

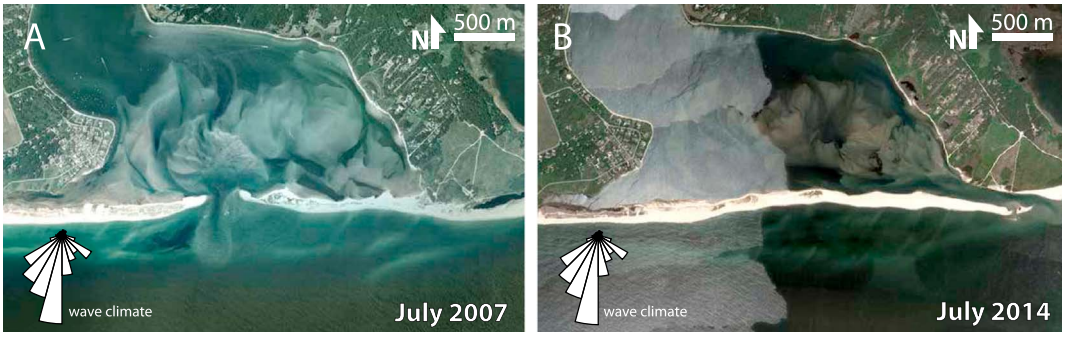

Figure 1. Katama inlet on Martha's Vineyard, MA in (a) July 2007 and in (b) July 2014, showing migration of approximately 2.5 km in 7 years. Wave rose shows the angular distribution of wave energy hindcasted using WaveWatch III® [*Chawla et al.,* 2013]. Images © Google Earth.

and the local inlet sediments control the size of tidal inlets; the potential tidal prism of the basin sets the spacing of tidal inlets along a barrier coast [*Johnson*, 1919; *O'Brien*, 1966; *Roos et al.,* 2013].

Tides move water and sediment into and out of the tidal basin and form flood-tidal and ebb-tidal deltas [*Hayes*, 1980]. Tidal basins are generally shallower than the open coast, spreading the flood-tidal jet more radially than the ebb jet, thus forming a flood-tidal delta with often complex channel patterns [*de Swart and Zimmerman*, 2009]. Waves strongly affect sediment transport around tidal inlets; tidal inlet morphology is therefore often considered a balance between tide-driven and wave-driven sediment transport [*Hayes*, 1980]. Waves limit the size of the ebb delta and create a water level setup along the open coast that generally moves sediment into the basin [*Walton and Adams*, 1977; *Dodet*, 2013]. Obliquely approaching waves and the associated alongshore current can affect ebb-tidal deltas by deflecting the ebb-tidal jet [*Stommel and Former*, 1952].

1.3. Tidal Inlet Migration

Forced by wave-driven littoral transport, many tidal inlets on barrier coasts migrate alongshore [*Johnson*, 1919]. For example, Oregon inlet in North Carolina has migrated 3 km southward since it formed in 1849, an average rate of 23 m yr^{-1} [*Inman and Dolan*, 1989]. Inlets can migrate rapidly; for example, Katama inlet in Massachusetts sustained an average migration rate of 375 m yr^{-1} between 2007 and 2014 (see Figure 1). Inlets can also migrate for long distances; Nauset inlet, Massachusetts, migrated 9 km alongshore between 1946 and 1987, at a rate of about 225 m yr^{-1} [*Giese*, 1988]. Tidal inlet migration away from its original breach location can lead to a decrease in the tidal prism if the flow gradually becomes less efficient because of basin infilling and tidal channel lengthening. Because the tidal prism is linked to the ability of inlets to maintain their size, an inlet can migrate itself to closure when the tidal currents become insufficient to erode the channel. Tidal inlet migration can also allow subsequent barrier breaches to take over and capture more of the potential tidal prism. A cycle of inlet formation, migration, and closure occurs in the Nauset barrier-inlet system on Cape Cod, where each cycle lasts approximately 150 years [*Giese*, 1988].

Investigating the mechanisms of tidal inlet migration, *Bruun* [1978] noted that tidal inlets tend to migrate in the direction of the littoral drift, with littoral sediment deposition updrift of the inlet and tidal-flow-driven erosion downdrift of the inlet. *Inman and Dolan* [1989] studied potential sediment pathways around Oregon Inlet, NC, and their relation to inlet migration. One of these pathways is alongshore sediment bypassing, where sediment is transported from the littoral zone updrift of the inlet to the littoral zone downdrift of tidal inlet. Alongshore sediment bypassing can occur via different mechanisms that each carry different morphologic expressions [*Oertel*, 1977; *Fitzgerald*, 1982]. Continuous bypassing can be wave driven along the ebb-tidal delta, or tide-driven through the inlet channel and the flood-tidal delta. Episodic bypassing pathways arise through the formation and migration of bypassing bars, where a sediment volume is instantaneously bypassed when a new ebb-tidal channel forms [*Fitzgerald*, 1982]. *Bruun and Gerritsen* [1959], modified by *Kraus* [2000], developed a bypassing parameter $r = P/M_{tot}$, where M_{tot} is the mean annual volume of littoral sediment transported toward the inlet ($m^3\,yr^{-1}$ of sediment) and P is the tidal prism (m^3 of water). Inlets that have low values of r ($r < 50$, littoral-transport-dominated inlets) tend to

bypass sediment along the ebb delta and are prone to inlet closure. For inlets with high values of r ($r > 150$, tidal-flow-dominated inlets), bypassing typically occurs via the channel [*Bruun and Gerritsen*, 1959; *Kraus*, 2000].

Littoral sediment that does not bypass the inlet can move through the channel and become part of the flood-tidal delta. Also, littoral sediment that is neither deposited in the flood-tidal delta nor bypassed can be deposited on the updrift barrier, leading to downdrift spit extension [*Inman and Dolan*, 1989]. In the analysis of *Inman and Dolan* [1989], they assumed that sediment eroded from the downdrift barrier can only flow into the littoral zone. However, *Hayes* [1980] and *Hine* [1975] analyzed bed forms in and around tidal inlets and observed current-related offshore export of sediment through the inlet channel and mixed tidal and wave-driven import of sediment along both inlet flanks.

1.4. Effect of Tidal Inlets on Barrier Islands

Tidal inlets and tidal inlet migration are tightly coupled to the dynamics of barrier islands [*de Vriend et al.,* 1994]. Inlets can act as a net sink of littoral sediment through flood-tidal delta deposition [*Hayes*, 1980; *Fitzgerald*, 1988], which can lead to erosion and thinning of downdrift barrier islands [*Inman and Dolan*, 1989; *Fenster and Dolan*, 1996]. In some environments, for example, the Texel Inlet in the Netherlands before the construction of the Afsluitdijk, tidal inlets can be ebb dominant and act as a source of sediment to the littoral zone [*Dastgheib*, 2012; *Ridderinkhof et al.,* 2014]. Wave dominance leads to straighter barrier coasts, whereas more tidally influenced coasts tend to develop "drumstick"-shaped barrier islands that curve inward around the inlet [*Hayes*, 1980]. Inlets also leave a sedimentological imprint on barrier islands [*Moslow and Heron*, 1978; *Moslow and Tye*, 1985; *Fitzgerald*, 1988]—geologic investigations suggest that as much as 50% of the Outer Banks of North Carolina was at one point a tidal inlet [*Mallinson et al.,* 2010]. Because of inlets' ubiquity and effectiveness as a sediment transport agent, *Moslow and Tye* [1985] conjectured that tidal inlets provide an important mechanism for barrier rollover, the long-term landward movement of barrier coasts. Despite their importance, however, the effect of tidal inlets on barrier islands remains poorly quantified and generalized. By examining inlets and inlet migration as a mass balance between the littoral zone and the lagoon, our study could help to quantify the long-term effect of inlets on barrier island evolution.

1.5. Models of Tidal Inlet Morphodynamics

Because of the engineering and management (dredging) challenges associated with tidal inlet dynamics, many numerical models have been developed that aim to capture the directions and magnitudes of sediment transport through inlets [e.g., *Bruun and Gerritsen*, 1959; *de Vriend et al.,* 1994; *Kraus*, 2000; *Tung et al.,* 2009; *Hoan et al.,* 2011; *Dodet*, 2013]. An essential element of many of these models is littoral sediment bypassing, and research has focused on the mechanisms and rates of transport of updrift littoral sediment to the littoral zone downdrift of the inlet system.

Kraus [2000] modeled alongshore sediment bypassing of tidal inlets in a "reservoir" model where the ebb- and flood-tidal deltas act as repositories for littoral transport brought into the tidal inlet. This model assumes that the fraction of alongshore sediment captured by both tidal deltas depends on the delta volume deficit relative to a natural equilibrium, such that all alongshore sediment will bypass the inlet when the ebb- and flood-tidal deltas are at equilibrium. Similarly, in a different model by *de Vriend et al.* [1994], alongshore sediment bypassing is dependent on the geometry of the ebb-tidal delta, such that littoral transport, bypassing, and the volume of the ebb-tidal delta tend to an equilibrium state. *Hoan et al.* [2011] estimate the fraction of updrift sediment that is able to bypass the inlet by the relative channel depth versus the breaking wave depth.

The alongshore sediment bypassing models of *Kraus* [2000] and *Hoan et al.* [2011] have been applied to models of spit growth and generally show good correspondence to stable (i.e., nonmigrating, mostly jettied) inlets or free, unrestricted spit growth. In *Hoan et al.* [2011] and *Kraus* [1999], the downdrift barrier is not erodible, which leaves these models unable to capture the interactions between bypassing and inlet migration. In this study we will suggest that inlet migration itself can change the volume of the ebb- and flood-tidal deltas, allowing for a rich dynamic not present in these static models.

Recent coupled hydrodynamic and morphodynamic models such as Delft3D [*Tung et al.,* 2009; *Dastgheib*, 2012], MORSYS2D [*Nahon et al.,* 2012], and SELFE [*Dodet*, 2013] show promising simulations of subaqueous tidal inlet dynamics, including ebb-tidal delta breaching and flood-tidal delta channel branching.

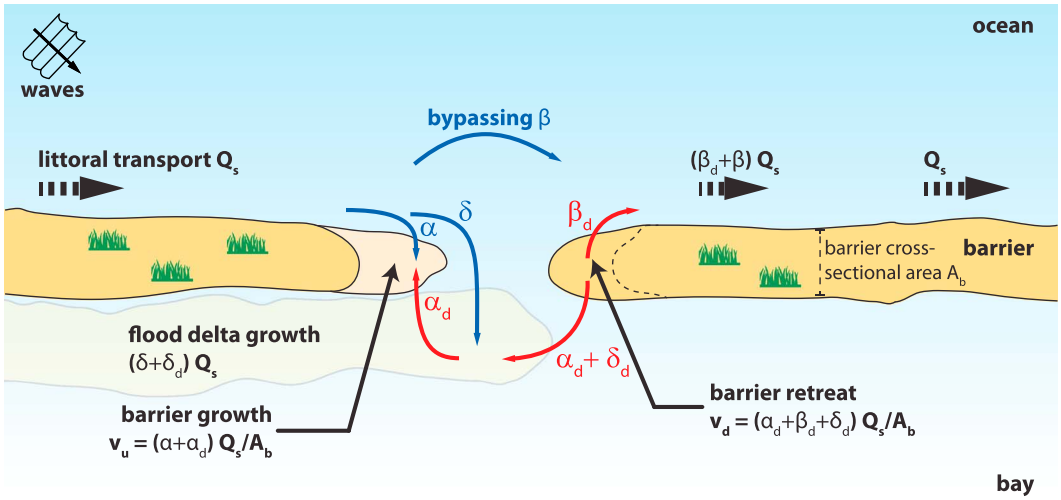

Figure 2. Plan view mass balance framework of tidal inlet migration. Sediment transport fluxes α, β, δ, α_d, β_d, and δ_d are normalized by the littoral transport Q_s to quantify the growth and retreat rate of the updrift and downdrift tidal inlet bank along a barrier coast.

Here we choose an approach similar to *Tung et al.* [2009]: we model tidal inlets with Delft3D-SWAN [*Deltares*, 2014] in an idealized environment to better understand and generalize inlet morphodynamics. Whereas *Tung et al.* [2009] studied littoral bypassing around a fixed equilibrium inlet, we focus on the morphodynamic interaction between bypassing and inlet migration. In a similar modeling framework, *Nienhuis et al.* [2016] investigated the coupling of alongshore sediment bypassing and alongshore river mouth migration.

1.6. Overview

We hypothesize that alongshore sediment bypassing of the tidal channel and flood-tidal delta deposition, both set by tidal inlet morphodynamics, are first-order controls on the mass balance of the tidal inlet and therefore control inlet migration rates at decadal timescales. The approach of this study is twofold. First, we use Delft3D-SWAN model experiments of tidal inlets to understand the physical mechanisms that lead to inlet migration. Next, we parameterize these model results within a mass balance framework of tidal inlet migration that we then apply to predict the migration rate of tidal inlets in natural settings.

In the following, we first present a mass balance framework of an idealized inlet to define how partitioning of sediment transport fluxes across a tidal inlet influences inlet migration and the downdrift barrier. We then present our Delft3D-SWAN model setup and analyze model results in terms of inlet morphology, sediment deposition, inlet migration mechanics and rates, and sediment flux partitioning. From these model experiments, we then formulate a parameterized model that predicts inlet migration rate based upon wave, tide, and basin characteristics. Finally, we compare our model predictions to observations of the migration rate of 22 inlets along the U.S. East Coast.

2. Mass Balance of a Migrating Inlet

To better understand the relationship between littoral transport and tidal inlet migration, we first propose a quantitative mass balance model for tidal inlets (Figure 2). This mass balance model schematizes the barrier coast by its cross-sectional area A_b (m^2): the deposited barrier volume for every meter of inlet migration. We consider two sources of sediment that can be supplied to a migrating tidal inlet, (1) the littoral sediment (Q_s, blue in Figure 2) and (2) the eroded barrier (red in Figure 2).

1. The long-term net alongshore sediment transport rate Q_s ($m^3\ s^{-1}$) feeding inlet migration is supplied from the updrift surf zone. For a given littoral flux Q_s transported toward the inlet, the bypassing fraction β describes littoral sediment that bypasses the inlet and joins the downdrift side of the barrier, a flood-tidal delta fraction δ ends up in the flood-tidal delta, and a barrier fraction α is deposited updrift of the inlet as barrier (Figure 2). Ensuring mass balance, α, β, and δ sum to 1.

2. The second source of sediment to a migrating tidal inlet is the eroded downdrift barrier. Sediment eroded from the retreating downdrift barrier can either continue to move downdrift into the littoral zone (at a rate of $Q_s \cdot \beta_d$) or be transported into the channel, in the latter case deposited either in the flood-tidal delta (at $Q_s \cdot \delta_d$) or as part of the updrift barrier (at $Q_s \cdot \alpha_d$). Note that as we have normalized these fluxes by the updrift alongshore sediment transport rate Q_s they therefore generally do not sum up to 1. This normalization, however, allows for straightforward comparison with the littoral sediment partitioning fractions α, β, and δ.

Based upon the proposed mass balance, the rate of updrift barrier migration into the inlet channel (v_u in $\mathrm{m\,s^{-1}}$) is as follows:

$$v_u = \frac{Q_s \cdot (\alpha + \alpha_d)}{A_b}, \tag{1}$$

and the rate of migration of the downdrift inlet bank (v_d, in $\mathrm{m\,s^{-1}}$) is as follows:

$$v_d = \frac{Q_s \cdot (\alpha_d + \beta_d + \delta_d)}{A_b}. \tag{2}$$

As a necessary condition, a migrating inlet channel will be in dynamic equilibrium (i.e., will maintain its width) when v_u and v_d are equivalent.

Note that this mass balance model does not prescribe any mechanisms or sediment pathways and that the fractions describe the volumetric fluxes of sediment transported to these various locations around the inlet. Even though the ebb-tidal delta likely plays an important role in the dynamics of migrating tidal inlets, we assume that the ebb-delta volume stays constant during inlet migration. Assuming that the ebb delta does not present a loss of sediment from the littoral system allows us to ignore the ebb delta volume in this formulation. An ebb delta reservoir could be added to a more detailed mass flux model in the future, in particular, for studies interested in shorter timescale inlet dynamics and channel dredging response. Additionally, this framework considers the mass balance of coarse-grained (littoral) sediment rather than fine-grained sediments.

The flood-tidal delta is gradually abandoned as the inlet migrates downdrift. An important consequence, therefore, is that, by migrating, inlets can act as a more efficient sink of littoral transport compared to a static inlet [*Inman and Dolan*, 1989]. The total volumetric sink flux out of the littoral system to the flood delta is Q_s $(\delta + \delta_d)$. If the accreted barrier and eroded cross-sectional areas A_b are equal and the flood-tidal delta grows, either the tidal inlet will widen ($v_d > v_u$) or the downdrift beach will erode ($\beta + \beta_d < 1$) (or both will occur). Inlets can be a net exporter of (coarse-grained) sediment if the flood-tidal delta volume decreases ($\delta + \delta_d < 0$), but such conditions are not found in this study.

Given the simplifications such as a net littoral transport (which in nature must be averaged over changing wave conditions) and averaging over ebb-tidal delta dynamics, this mass balance model is more appropriate over yearly to decadal timescales, similar to the timescales of inlet migration. The view of bypassing here is Lagrangian, defined at the inlet location: the fraction of alongshore sediment that is bypassed depends on the location of the inlet.

3. Methods

To test the mass balance framework proposed above, we model alongshore sediment bypassing, flood-tidal delta deposition, and tidal inlet migration in an idealized barrier environment with the process-based coupled hydrodynamic and morphodynamic model Delft3D-SWAN [*Deltares*, 2014]. This idealized model setup does not simulative any particular barrier-inlet environment in detail, allowing us to investigate a wide range of idealized geometries and boundary conditions that broadly represent migrating inlets globally. We then use parameterizations based on these model experiments to make predictions of observed tidal inlet migration rates. This approach can be viewed as a hybrid exploratory-simulation method: we apply a simulation model (Delft3D-SWAN) with both exploratory model goals (understanding inlet migration processes) and simulation model goals (quantifying natural inlet migration rates) [*Murray*, 2007].

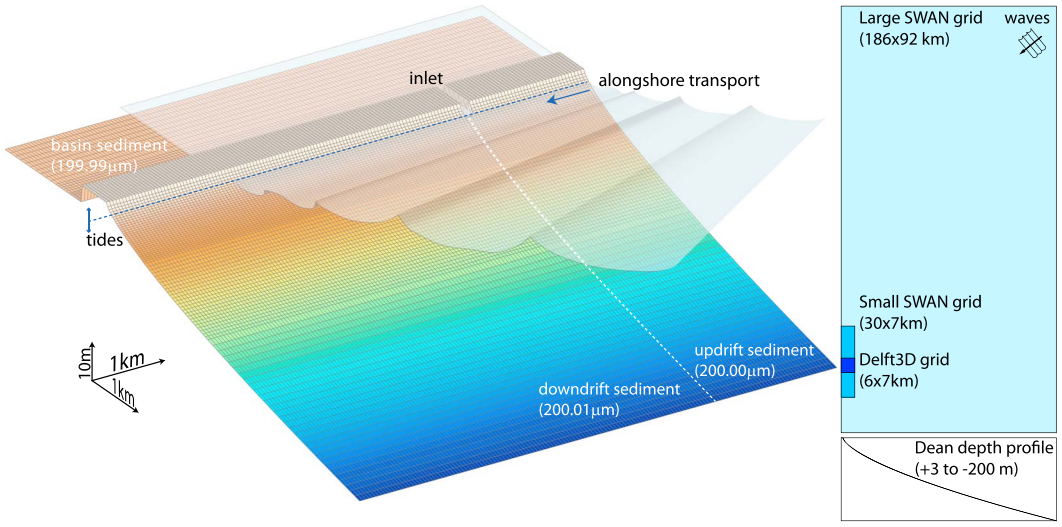

Figure 3. Delft3D flow model setup. The insets show the large and small SWAN wave grids that provide wave forcing conditions for the flow model and the shoreface profile for the flow and wave domain.

3.1. Delft3D-SWAN

We use Delft3D in the 2DH mode to compute depth-averaged flows from the shallow-water equations. Using bed load and suspended load transport formulas from *van Rijn* [1993], Delft3D also calculates morphologic change in response to imposed boundary conditions. We embed the Delft3D flow model into the SWAN phase-averaged spectral wave model that uses the wave action equation to simulate wave refraction, wave dissipation, and wave-current interaction [*Booij et al.,* 1999]. See supporting information Table S1 for an overview of all the model parameters. For a detailed description of the model formulations and model implementation, see *Deltares* [2014].

3.2. Model Setup

The initial bathymetry of the flow domain consists of a 6 km long coastal barrier, a tidal basin, and an open coast with parallel depth contours that follow a Dean profile [*Dean*, 1991], extending to 27 m water depth (Figure 3). The flow domain consists of 132 cells in the cross-shore direction that range from 100 m wide at 5 km offshore to 25 m wide close to the barrier. In the alongshore direction there are 152 cells of 40 m. A tidal inlet simulation with a finer grid resolution shows nearly identical morphodynamics (supporting information Figure S1).

The offshore boundary condition is set by an M_2 tide water level, with a tidal range that varies between 0.6 m and 2 m between the different experiments. The tidal wave is normally incident. Although alongshore propagating tides may affect inlet morphodynamics and migration, tidal waves may or may not be in the direction of wind and swell waves. We choose to simplify our approach and consider only the alongshore current driven by obliquely approaching waves.

Neumann conditions are prescribed at the alongshore boundaries to allow water and sediment to flow through the domain. The boundary on the bayside of the barrier is closed (no flow). Between the model experiments we vary the barrier width from 100 m to 800 m, the basin depth between 1 m and 5 m, and the basin size from 8.4 to 17.4 km^2. The initial inlet is 4 m deep and 120 m wide. The flow domain is embedded into two wave domains of which the largest extends 186 km alongshore and 90 km offshore, up to 200 m water depth (Figure 3). A wave domain of this size prevents boundary artifacts from reaching the flow domain and allows obliquely approaching deep water waves to fully develop an alongshore current [*List and Ashton*, 2007].

Waves are prescribed at the offshore and updrift wave domain boundary and approach at 40° from shore normal with a 10° directional spread (Figure 3) and a JONSWAP frequency spectrum. We vary significant wave heights from 0.8 m to 1.2 m and peak wave periods from 8 s to 10 s. Wave-induced radiation stresses drive an

alongshore current in the flow domain. There is no local regeneration of waves by wind—therefore, sediment in the tidal basin can only be transported by tidal currents or incidental waves that make it through the inlet. See supporting information Table S2 for an overview of all experimental parameters.

After 1 day of hydrodynamic spin-up, we run the morphodynamic model for 28 days. Every time step (12 s), we scale the computed vertical morphologic change using a scaling factor of 90 to speed up the morphodynamics. The 28 hydrodynamic days with 56 tidal cycles approximate a total of 7 years of morphologic change. Tests with morphological factors of 10 and 45 showed nearly identical resulting morphologies (see supporting information Figure S2). However, a slight increase (5%) in the migration rate of the tidal inlets was observed for smaller morphologic scaling factors, likely due to the more frequent (in morphologic time) updating of the wavefield in the SWAN model. Note that in our study we are examining long-term (decadal) tidal inlet dynamics—even though morphologic change during each tidal cycle is greatly exaggerated, our tests with different morphologic factors indicates that this exaggeration does not affect the long-term modeled tidal inlet characteristics and behavior.

During the morphologically active part of the simulation, grid cells can become dry due to sedimentation or water level lowering, at which point it can no longer receive sediment. All new land in Delft3D is therefore created up to the high-tide water level. A dry cell erodes if erosion occurs in a neighboring wet cell, at which point a fraction of the wet cell erosion is assigned to the dry cell. We set this fraction to 0.8 following a Delft3D modeling study of tidal inlets by *Tung et al.* [2009].

The model tracks the sediment composition of each grid cell using 25 vertical layers of 20 cm. We divide the initial bed composition into three classes of sediment: one "updrift" class of 200.00 μm sand initially located in the updrift ocean part of the domain, one "downdrift" class of 200.01 μm sand, and one "basin" class of 199.99 μm sand basinward of the barrier (Figure 3). Modeled in this way, sediment acts as a tracer while keeping the sediment transport properties nearly identical, allowing us to track the fraction of updrift and downdrift sediment migrating past the tidal inlet and eventually deposited in various locations [*Nienhuis et al.*, 2016].

3.3. Model Analyses

For each model experiment, we investigate tidal inlet morphodynamics and the sediment transport fractions α, β, δ, α_d, β_d, and δ_d (Figure 2). We compute these transport fractions by tracking the location of the inlet through time. We then sum the volumes of the different classes of sediment located in different parts of the model domain. These volumes divided by the cumulative volume of updrift littoral sediment brought into the model domain along the updrift boundary result in cumulative sediment transport fractions. All of the 200.00 μm "updrift" sediment that is located downdrift of the inlet and seaward of the tidal basin, including sediment that has left the domain on the downdrift boundary, is summed and divided by the cumulative littoral sediment flux Q_s to provide the cumulative bypassing fraction β. All of the 200.00 μm "updrift" sediment that is located basinward of the original barrier island adds to the cumulative flood-tidal delta fraction δ. The remainder of the updrift littoral sediment flux, either on or seaward of the barrier updrift of the inlet, constitutes the cumulative barrier fraction α.

We also track the 200.01 μm sediment eroded from the downdrift barrier to compute the fractions α_d, β_d, and δ_d (Figure 2): δ_d is the total volume of the "downdrift" sediment that is deposited in the basin, and α_d is the volume of "downdrift" sediment that is updrift of the tidal inlet, seaward of the basin and located above the maximum eroded surface of the tidal inlet. The last fraction β_d is calculated by summing the change in "downdrift" sediment volume across the downdrift barrier, including the sediment that has left the domain.

4. Morphology of a Migrating Inlet

In our model experiments of migrating inlets, we find that alongshore sediment transport and tidal inlets quickly reach a dynamic steady state resulting in a roughly constant tidal prism, inlet cross-sectional area, ebb-tidal delta volume, and inlet migration rate through time (e.g., Figure 4 and Animation S1). These inlet properties arise from the boundary conditions and barrier geometry chosen for each model experiment, and their steady behavior is critical as it indicates that the dynamics of interest are emergent characteristics of the underlying model dynamics rather than model spin-up or morphologic time step artifacts. This dynamic steady state also shows that we have chosen a sufficiently long simulation period and allows us

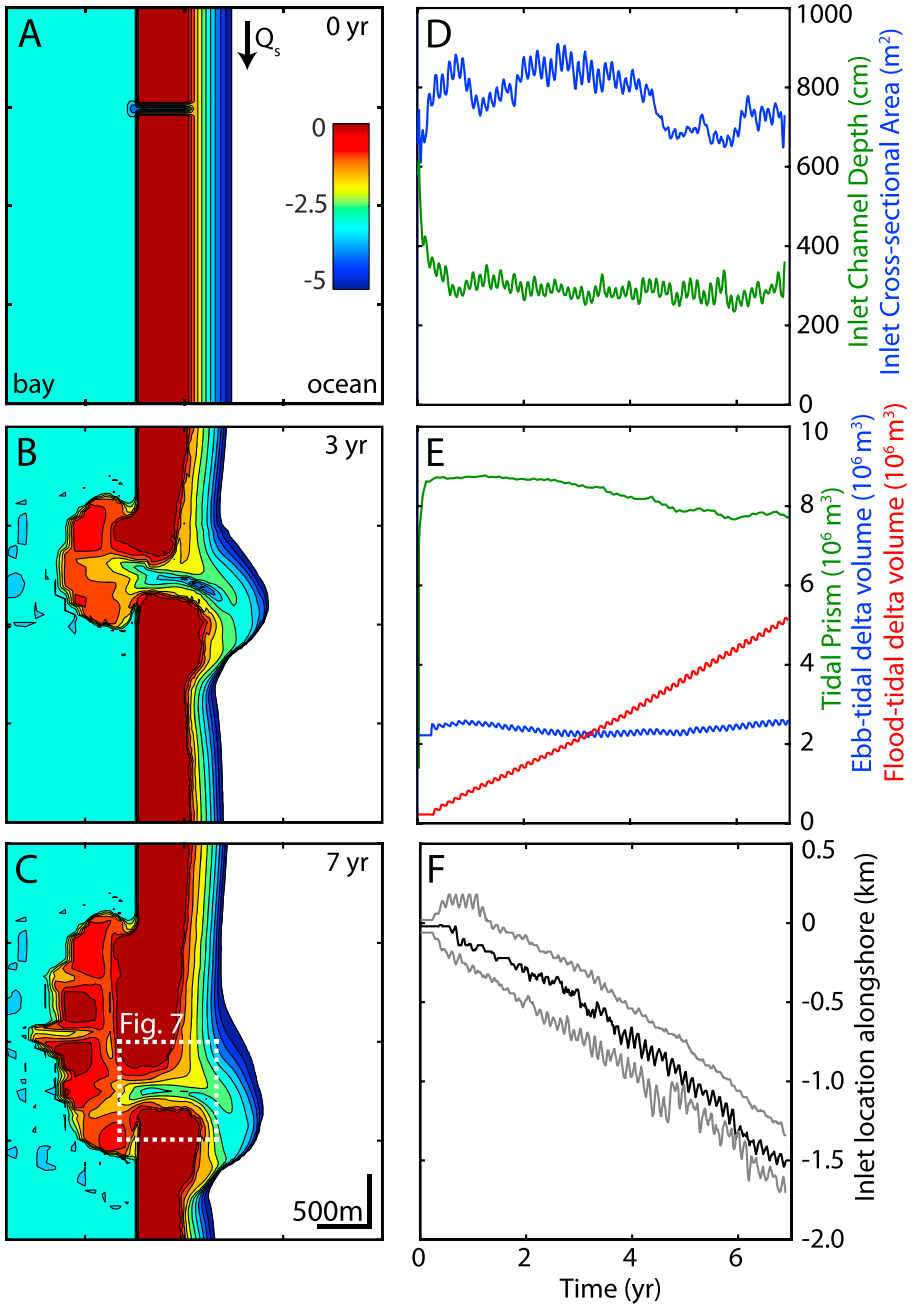

Figure 4. Model experiment of a migrating inlet showing bathymetry after (a–c) 0, 3, and 7 model years, respectively, (d) inlet channel depth and inlet cross-sectional area through time, (e) tidal prism, ebb-tidal, and flood-tidal delta sediment volume through time, and (f) location alongshore of the inlet thalweg (black) and the inlet updrift and downdrift banks (grey) through time. H_s = 1.2 m, T_p = 10 s, M_2 tidal range = 1 m. See supporting information Table S2, model experiment #7.

to seek a description of tidal inlets where the sediment distribution fractions converge to constant values and can be linked to the inlet environment.

A close examination of the morphology of one model experiment (Figure 4) shows the development of the ebb-tidal and flood-tidal deltas. The ebb-tidal delta shares characteristics commonly found in wave-dominated environments, with a single ebb channel deflected away from the incoming waves [*Sha and van den Berg*, 1993]. The volume of the ebb-tidal delta, defined in this model experiment as the total shoreface sediment volume above the reference cross-shore bathymetry [*van der Vegt et al.*, 2006], is ~2.5×10^6 m^3.

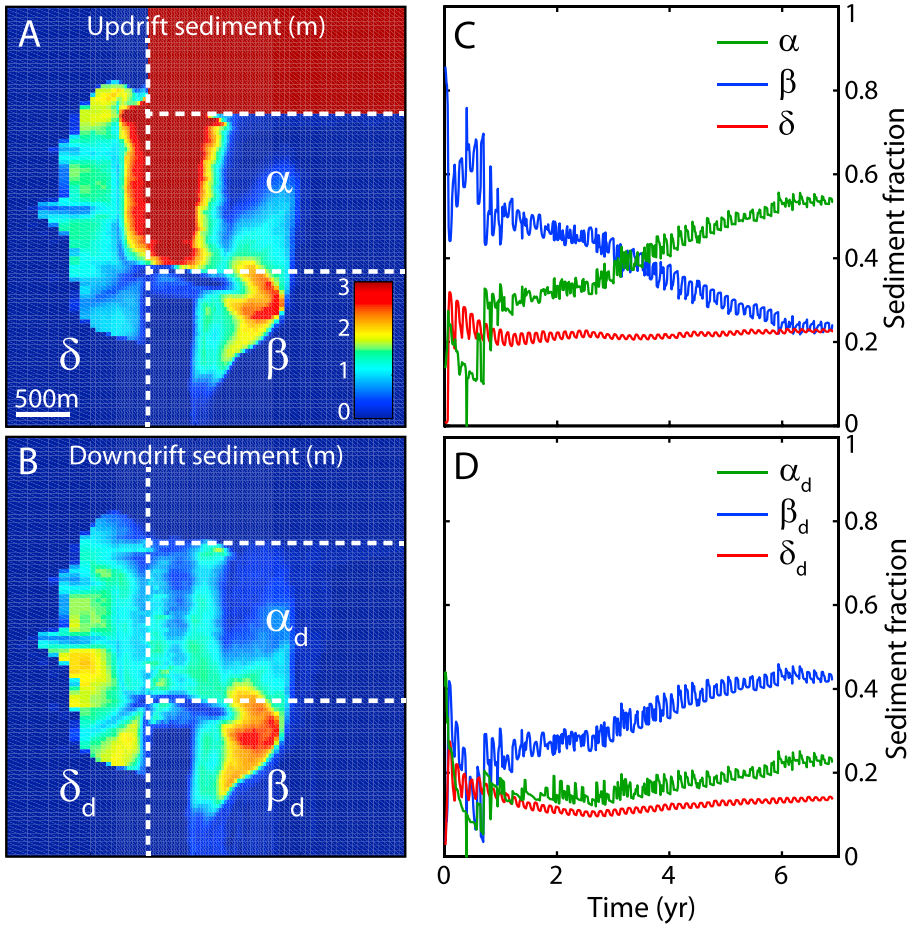

Figure 5. Distribution of (a) updrift sediment and (b) downdrift sediment in the model experiment of Figure 4 after 7 years of morphologic change. Colors indicate deposit thickness in meters. Dashed lines separate the barrier environments for calculating the respective sediment partitioning fractions. (c) Cumulative littoral sediment partitioning fractions over the course of the experiment. (d) Eroded downdrift inlet bank sediment partitioning fractions. Model experiment #7.

This volume is consistent with *Walton and Adams* [1977], who, for moderately exposed inlets, predict the ebb-tidal delta volume $V_{ebb} = 0.00643\,P^{1.23} = 2.0 \times 10^6\,m^3$, where P is the tidal prism (m^3). The flood-tidal delta is larger than the ebb-tidal delta, also a characteristic of wave dominance. The inlet migrates at a rate of approximately 220 m yr^{-1} and deposits a barrier with a roughly constant cross-sectional area (A_b, inlet depth multiplied by barrier width) of 1500 m^2, leaving behind flood-tidal delta deposits, while the ebb-tidal delta migrates with the inlet (Figure 4).

By summing the volume of updrift and downdrift sediment transported in and around the tidal inlet, we can investigate how littoral sediment supply and downdrift barrier erosion contribute to inlet migration. For the experiment shown in Figure 5, 22% of the littoral sediment flux transported to the inlet is bypassed ($\beta = 0.22$), either through the channel or around the ebb-tidal delta. A similar fraction of the littoral sediment flux is brought into the inlet and deposited in the flood-tidal delta ($\delta = 0.22$). The remainder of the littoral sediment flux is deposited on the updrift flank of the inlet as barrier island ($\alpha = 0.56$).

As the downdrift inlet bank erodes, a flux of $Q_s \cdot \delta_d$ is deposited in the flood-tidal delta, and a flux of $Q_s \cdot \beta_d$ is transported into the littoral zone. δ_d and β_d sum up to approximately α, leading to equal barrier progradation and erosion ($v_u \sim v_d$ from equations (1) and (2)), and a roughly constant of inlet width and depth (Figure 4d). The sediment supply into the flood-tidal delta (the net sink of littoral sediment, $\delta_d + \delta = 0.36$) is therefore mainly driven by sediment loss from the downdrift littoral zone ($\beta + \beta_d = 0.64 < 1.0$). However, similar to observations by *Bruun and Gerritsen* [1959], our model experiment shows a relatively wide barrier immediately downdrift of the inlet. The sediment deficit only becomes apparent farther downdrift, where the barrier

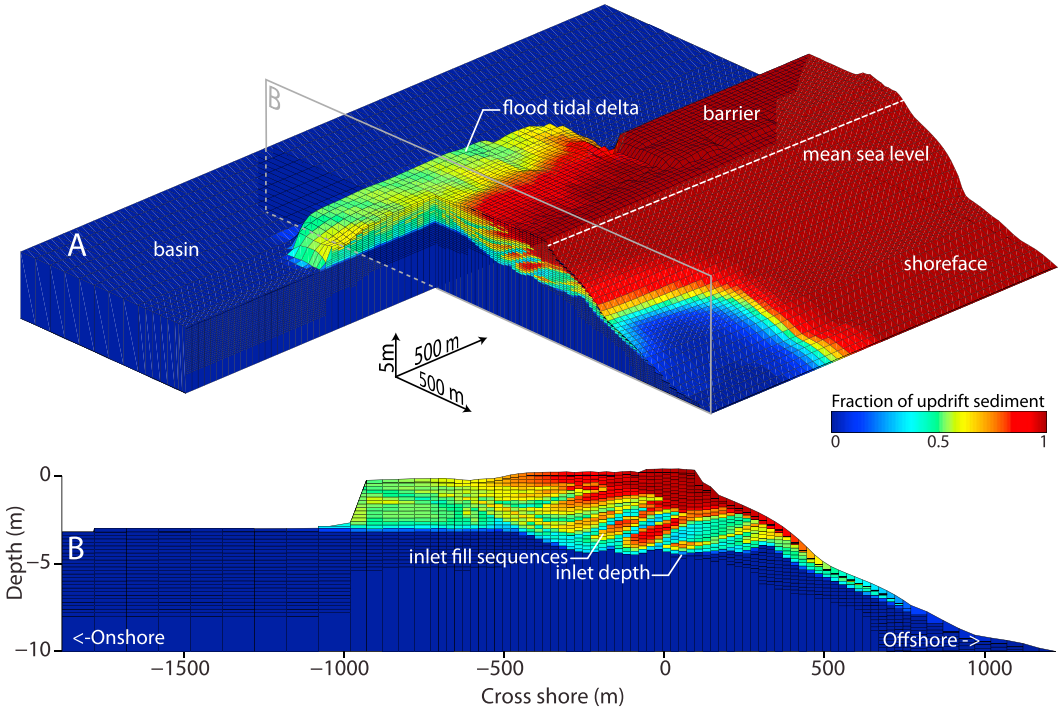

Figure 6. (a) Volumetric slice through the constructed barrier and flood-tidal delta of the experiment illustrated in Figures 4 and 5 after 7 years of morphologic change. Colors indicate the fraction of updrift sediment, and the perspective view is lagoonward and updrift. Perspective box indicates cross section of Figure 6b. (b) Cross section of the constructed barrier and flood-tidal delta.

shoreline erodes (Figure 4c). The migration rate of the simulated inlet is 217 m yr^{-1}, close to the computed value v_u (equation (1)) of 199 m yr^{-1}.

5. Inlet Sediment Provenance

The sediment pathways through our modeled tidal inlet can be observed by looking at the depositional architecture composed of "updrift" and "downdrift" sediments (Figure 6). Sediment transported from the updrift littoral zone combines with sediment eroded from the downdrift barrier to create a well-mixed flood-tidal delta with approximately 60% δ and 40% δ_d. The updrift barrier is constructed from both the littoral zone during flood (forming deposits that contain 90% updrift sediment, Figure 6) and the flood-tidal delta during ebb (forming deposits that contain 60% updrift sediment), resulting in a gross updrift fraction $\alpha/(\alpha+\alpha_d)$ of about 0.75. The remaining 25% of the newly formed barrier consists of sediment that originated from the eroded downdrift bank and subsequently was recirculated through the channel and the flood- and ebb-tidal deltas.

Studies of bed form directionality of inlet fill sequences have found bidirectional tidal bedding, indicating sediment deposition during both ebb and flood flow [*Kumar and Sanders*, 1974; *Hayes*, 1980]. However, because updrift and downdrift barriers are likely composed of similar sediments, bed form direction alone is insufficient to determine whether the sediment is originally from the littoral zone or from the eroded bank of the inlet. Model experiments such as ours show tidal bedding, which can inform stratigraphic studies by coupling bedding sequences to sediment sources. Note that the morphologic scaling factor used to speed-up morphologic change also creates scaled tidal bedding thicknesses, which for natural tidal inlet fill sequences is on the order of centimeters [*Hayes*, 1980], but for our model experiment are about 1 m thick (Figure 6a).

6. Mechanics of Inlet Migration

Migration of tidal inlets has long been understood to occur through gradual littoral sediment deposition on the updrift barrier and erosion of the downdrift barrier [*Bruun*, 1978]. However, the mechanisms

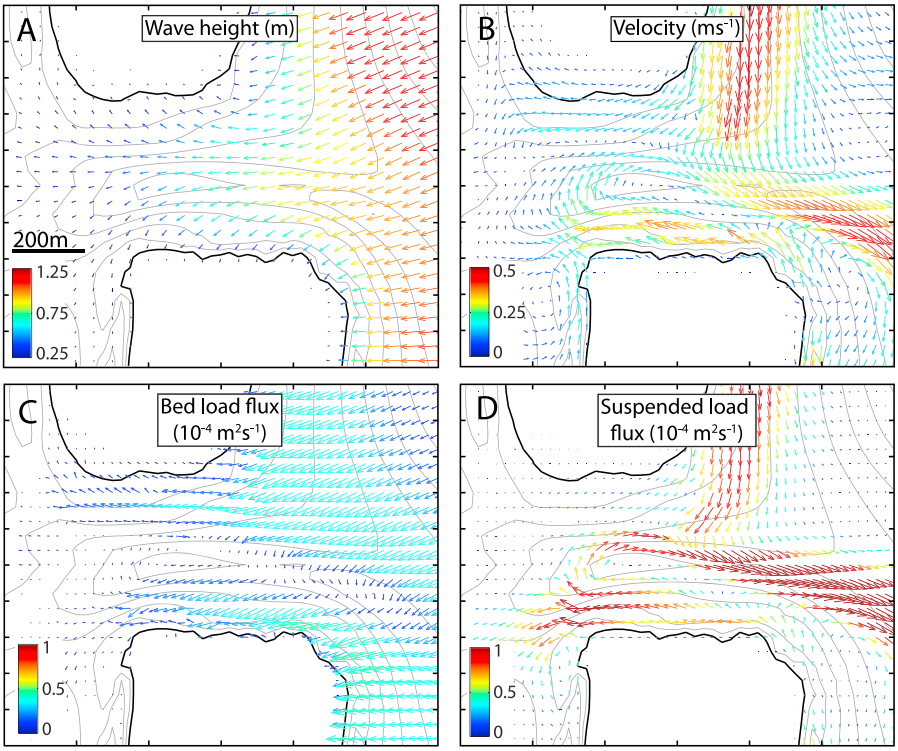

Figure 7. Tidally averaged (a) wave height and direction, (b) flow velocity, (c) bed load transport, and (d) suspended load transport for the model experiment shown in Figure 4. Gray lines indicate 0.5 m bathymetric contours between 0 m and 5 m below mean sea level; black line is sea level.

whereby littoral sediment transport would result in barrier migration are largely unknown. In our detailed hydrodynamic and morphodynamic simulations, inlet migration itself is an emergent characteristic of the model dynamics, allowing us to investigate the processes that drive tidal inlet migration.

Averaged over one tidal cycle, the model experiment shows that net sediment transport (and flow) is into the basin near the inlet boundaries and directed outward along the main channel (Figure 7). Wave-driven bed load transport is directed into the inlet and is on average about 5 times smaller than the wave- and current-generated suspended load flux (Figures 7c and 7d). These sediment transport mechanisms and directions are consistent with field studies of bed form orientation which indicate wave-driven net sediment import into the inlet along the flanks and current-driven net sediment export through the inlet channel [*Hayes*, 1980; *Komar*, 1996].

In our experiment, the tidally averaged sediment transport rate on the updrift side decreases into the inlet, which leads to deposition. The opposite is true on the downdrift inlet bank, where increasing sediment transport into the inlet leads to erosion (Figure 7d). Because tidally driven currents in the model should be symmetric in the absence of waves, we suggest that asymmetry in the sediment transport between the inlet banks is partially due to the direction of incoming waves, as impinging waves aid erosion of the downdrift bank and set up an alongshore current. Additionally, ongoing inlet migration leads to asymmetry of the flood-tidal delta: flow around the downdrift bank is less impeded by the shallow flood-tidal delta. Therefore, asymmetry in the flood-tidal delta deposits also affects inlet migration.

Investigating the currents, waves, and related sediment transport suggests that the tidal inlet migrates because of (1) preferential wave attack on the exposed downdrift flank (Figure 7a), (2) inertia of the alongshore current (Figure 7b), and (3) asymmetry in the tidal flows due to the asymmetry of the flood-tidal delta deposits (Figure 7b). These three factors lead to asymmetry in the suspended sediment transport about the inlet banks (Figure 7d) and cause inlet migration.

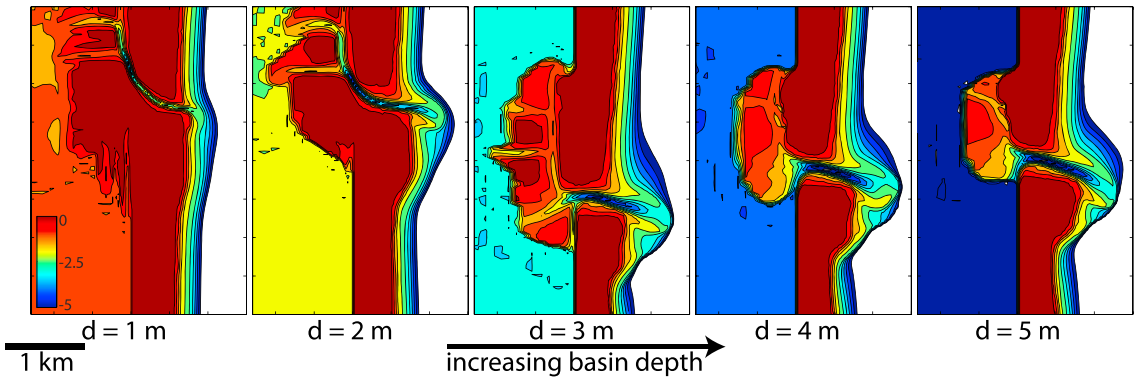

Figure 8. Bathymetry for model experiments with increasing (initial) basin depth (d) with similar tidal range, barrier width, and wave climate after 7 years of morphologic change. See supporting information Table S2, model experiments #7, 9, 10, 11, and 12.

7. Controls on Inlet Migration

Aside from investigating the mechanics of inlet migration, model experiments in Delft3D allow us to expand our analysis to study how antecedent geology and external driving conditions affect inlet morphodynamics. We ran 23 model experiments for a variety of wave and tidal conditions as well as barrier and basin properties (see supporting information Table S2). In general, our barrier island environments range from mixed-energy tide-dominated to the wave-dominated regime [*Hayes*, 1979]. All of the modeled inlets are net importers of littoral sediment into the bay.

Investigating tidal inlet morphodynamics for these scenarios, we find that basin depth exerts an important control on inlet migration rate (Figure 8). For shallow basins, flow through flood-tidal delta channels is constricted, which decreases the tidal prism and increases alongshore sediment bypassing—bypassing is high and the tidal inlet migration rate is low. On the other hand, a deep basin (with similar depths as the inlet channel) can easily accommodate flood-tidal delta deposits and flood-tidal delta channels. However, in this case, flood-tidal deltas are slower to redirect tidal flow that will push the inlet to migrate—tidal inlet migration is also low even as bypassing is limited. Even though for basin depths of 2, 3, 4, and 5 m the fraction of alongshore sediment transport deposited as flood tidal delta is roughly equal ($\delta = 0.2$), we observe the fastest migration rate for a basin of intermediate depth. This intermediate depth is deep enough for tidal channels not to be constricted but shallow enough for rapid flood-tidal delta expansion that modifies tidal flow around the downdrift bank (Figure 8).

In a set of experiments where we vary the barrier width, we find that tidal inlets migrate faster with narrow barriers (Figure 9). This is perhaps not surprising because the barrier width is linearly related to the barrier cross-sectional area A_b, which acts as an important control on the migration rate (equations (1) and (2)). Varying the tidal range, we find that it affects not only the migration rate but also the morphology of the deposited barrier. For high tidal range and narrow barriers, the updrift barrier spit curves inward forming a drumstick-like barrier updrift of the inlet (Figure 9) [*Hayes*, 1980]. The deposited barrier becomes less affected by the retreating barrier and attains a shape resembling that of a recurving, free spit [e.g., *Ashton et al.*, 2016].

In one model experiment, with low tidal range and a wide barrier, high friction in the channel resulted in inlet closure (Figure 9, bottom row right). Closure of this inlet is expected based on the bypassing parameter r of 11 which is less than 50 [*Bruun and Gerritsen*, 1959]. However, based on the closure criterion developed for non-migrating, mostly jettied inlets ($r < 50$) [*Kraus*, 2002], we find that all but two of our tidal inlet experiments are expected to close (supporting information Table S2). We hypothesize that by migrating, the flood-tidal delta never reaches its "equilibrium" volume, such that tidal inlets can stay open even if $r < 50$.

8. Sediment Flux Partitioning

The analyses thus far have been mostly qualitative, describing tidal inlet morphodynamics and environmental dependence. Using the framework presented in section 2, we can quantify tidal inlet migration based on how littoral sediment and eroded downdrift bank sediment are partitioned around tidal inlets. Then, by establishing dependencies between the inlet environment (characteristics that can be measured in the field)

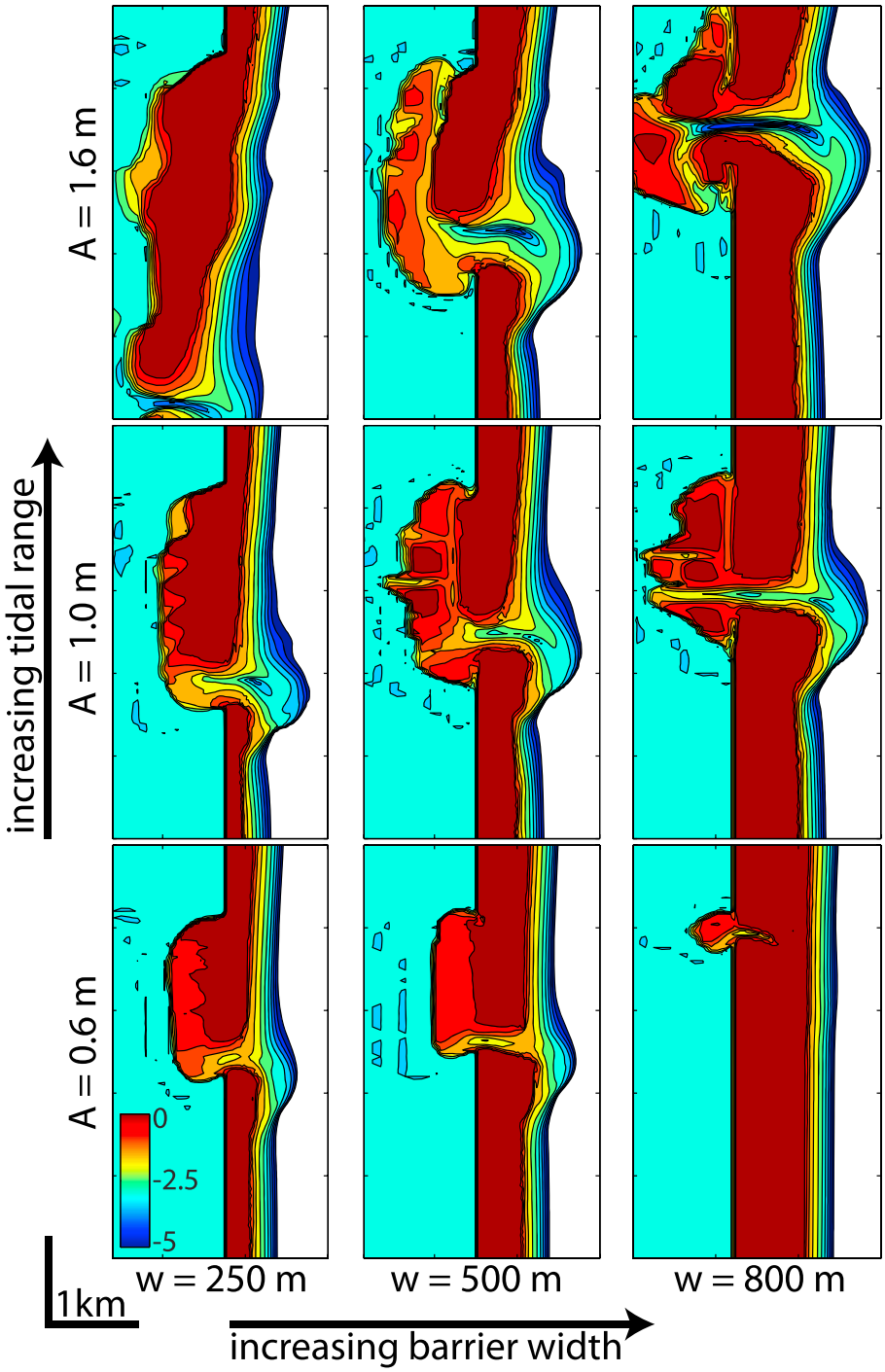

Figure 9. Bathymetry of model experiments after 7 years for tidal ranges of 0.6, 1.2, and 2.0 m, and barrier widths of 250 m, 500 m, and 800 m. See supporting information Table S2, model experiments #1, 2, 3, 6, 7, 8, 15, 16, and 17.

and sediment partitioning (which we can extract from model experiments), we can formulate predictive relations for tidal inlet migration rates.

8.1. Littoral Flux Partitioning

As littoral sediment from the updrift coastline is transported toward the inlet, it is distributed between fractions α, β, and δ. Our model experiments cover a wide range of these values (Figure 10). For some

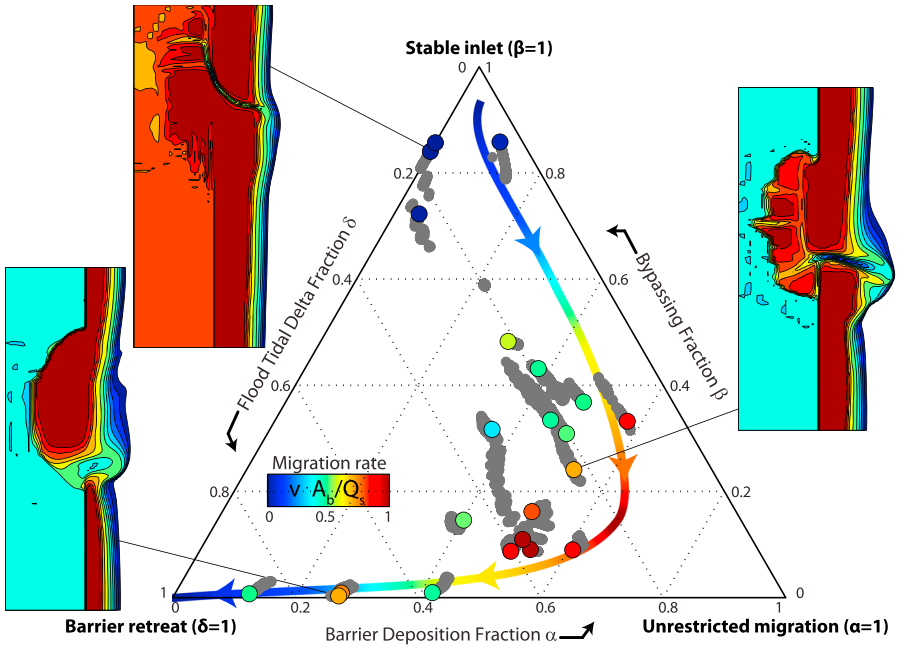

Figure 10. Ternary diagram of littoral sediment partitioning (fractions α, β, and δ) for all model experiments. The marker colors indicate the nondimensionalized 7 year inlet migration rate. Grey markers are the cumulative fractions taken every 18 min throughout the model experiments. The colored line displays the predicted migration rate assuming $\alpha_d = 3/5\alpha$, for increasing tide dominance (equation (5)). See supporting information Table S2; insets show plan views of model experiment #7, 9, and 20.

experiments, most sediment is bypassed ($\beta = 0.9$), whereas other experiments show a predominance of flood-tidal delta deposition ($\delta = 0.9$). If all of the littoral sediment bypasses the inlet ($\beta = 1$), the inlet will not migrate. On the other hand, the updrift barrier retreats if all the littoral sediment ends up in the flood-tidal delta ($\delta = 1$, the deposited barrier will be completely basinward of the original barrier). For $\alpha = 1$, all littoral sediment contributes to barrier migration, such that there is unrestricted growth of the updrift barrier spit [e.g., *Hoan et al.*, 2011].

8.2. Eroded Barrier Partitioning

Similar to the littoral sediment transported toward the inlet, sediment eroded from the downdrift inlet bank also partitions itself between the basin, barrier, and the littoral zone. Because the fractions α_d, β_d, and δ_d do not necessarily sum to unity, a ternary diagram is less applicable. Instead, we compare how eroded barrier partitioning relates to littoral sediment partitioning (Figure 11). For sediment deposited on the newly formed barrier, we find a positive relationship between sediment originating from the littoral zone (α) and sediment

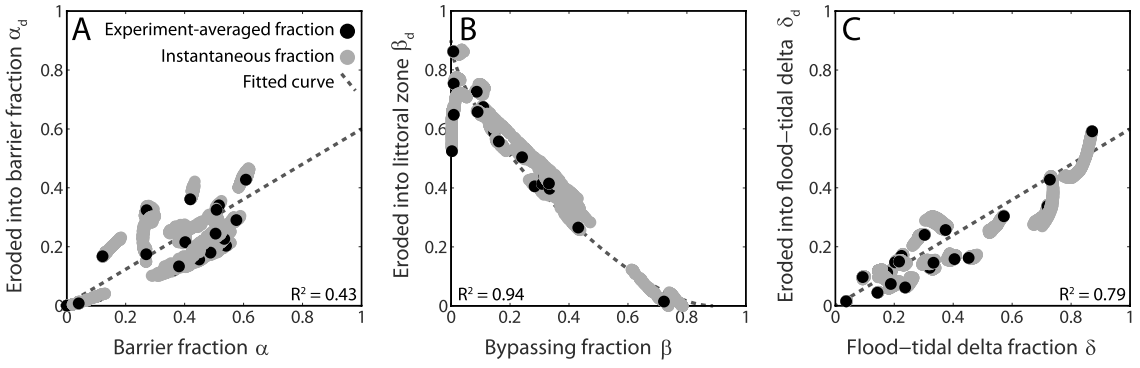

Figure 11. Relationships between the partitioning of littoral sediment (α, β, and δ) and the fraction of eroded barrier sediment deposited (a) in the newly formed barrier (α_d), (b) in the littoral zone downdrift of the inlet (β_d), and (c) in the flood-tidal delta (δ_d). The dashed lines indicate the fitted trends (equation (6)).

from the eroded barrier (α_d). The fraction of barrier deposition α increases with α_d because rapid migration also results in large volumes of eroded barrier sediment.

Alongshore sediment bypassing β and the proportion of eroded barrier that is transported into the littoral zone β_d are negatively correlated: bypassed littoral sediment does not contribute to inlet migration and downdrift bank erosion. β_d will tend to compensate for changes in β, placing an upper limit on the ability of inlets to act as a sink of littoral sediment transport (Figures 2 and 11b).

The contributions to the flood-tidal delta, δ and δ_d, are also correlated (Figure 11c). For tidal inlets where a large proportion of the littoral sediment is deposited in the flood-tidal delta, the eroded barrier is also preferentially deposited in the barrier. The relatively linear relationship points to a relatively constant proportion of littoral versus eroded barrier sediments in flood-tidal delta deposits.

9. Controls on Sediment Flux Partitioning

Our model experiments show that the partitioning of sediment in and around tidal inlets is an important control on barrier island morphology and tidal inlet migration rates (Figure 10). Thus, if we know how the sediment partitioning fractions α, β, δ, α_d, β_d, and δ_d vary across different environments, we can potentially forecast the migration rate and morphologic evolution of natural tidal inlets.

Tidal inlet morphology has long been considered a function of the local environment, in particular, depending on the tidal range and wave power [*Hayes*, 1979; *Hubbard et al.,* 1979]. Investigating 67 inlets in Florida, *Powell et al.* [2006] found that flood-tidal delta volumes increase with increasing tidal prism and decrease with increasing wave energy. In our model experiments, we also found that high tidal ranges lead to extensive flood-tidal delta growth (high δ, Figure 10). *Bruun and Gerritsen* [1959] found an opposite relationship for alongshore sediment bypassing, where bypassing volumes tend to increase with increasing littoral transport and decrease with increasing tidal prism. Because the barrier fraction α (=$1-\beta-\delta$) is large when neither bypassing nor flood-tidal delta deposition is large, we expect inlet migration to be maximum for mixed tidal and wave energy environments.

To formulate a predictive relationship of the nondimensional sediment partitioning fractions, we cast the opposing effects of wave energy and tidal prism into a nondimensional ratio of the relative momentum flux of currents into and out of the inlets (the tides, M_t) versus the momentum flux acting across this current (the waves, M_w) over the width of the inlet. Given the observations on how flood-tidal delta and bypassing volumes vary across different environments [*Bruun and Gerritsen*, 1959; *Powell et al.,* 2006], we expect M_t/M_w to be low for inlets with high β, medium for inlets with high α, and high for inlets with high δ.

We quantify the magnitude of tides by the depth- and width-integrated inlet momentum flux M_T (kg m s^{-2}):

$$M_T = \rho_w \cdot Q_{\text{ebb}} \cdot u, \tag{3}$$

where ρ_w is the water density (kg m^{-3}), Q_{ebb} is the maximum tidal inlet ebb discharge (m^3 s^{-1}), and u is the depth- and width-averaged ebb-tidal inlet velocity (m s^{-1}). We can also quantify the effect of waves on alongshore sediment bypassing by the alongshore component of the wave-momentum flux acting across the width of the inlet M_W (kg m s^{-2}),

$$M_W = S_{sy} \cdot W_{\text{inlet}} = E \cdot n(\cos\theta \cdot \sin\theta) \cdot W_{\text{inlet}}, \tag{4}$$

where S_{xy} is the alongshore directed component of the radiation stress (N m^{-1}) and W_{inlet} is the inlet width (m). E is the wave energy density (N m^{-1}) which equals $\frac{1}{16}\rho_w \,.\, g \,.\, {H_s}^2$ [*Airy*, 1841], g is the vertical acceleration due to gravity (m s^{-2}), H_s is the significant wave height (m), n is the ratio of the group velocity and the phase velocity of the incoming (deep water) waves, and θ is the incoming wave angle.

We find that the ratio of M_t to M_w alone does a poor job of explaining the variability in inlet sediment partitioning without accounting for the width of the barrier. We hypothesize that geometrically, the width of the barrier exerts an important control on sediment partitioning because the migration rate of the inlet (proportional to $1/W_{\text{barrier}}$) changes the rate of growth of accommodation space in the tidal basin for the flood-tidal delta (proportional to W_{inlet}). We therefore adjust the ability of the inlet to migrate by the ratio

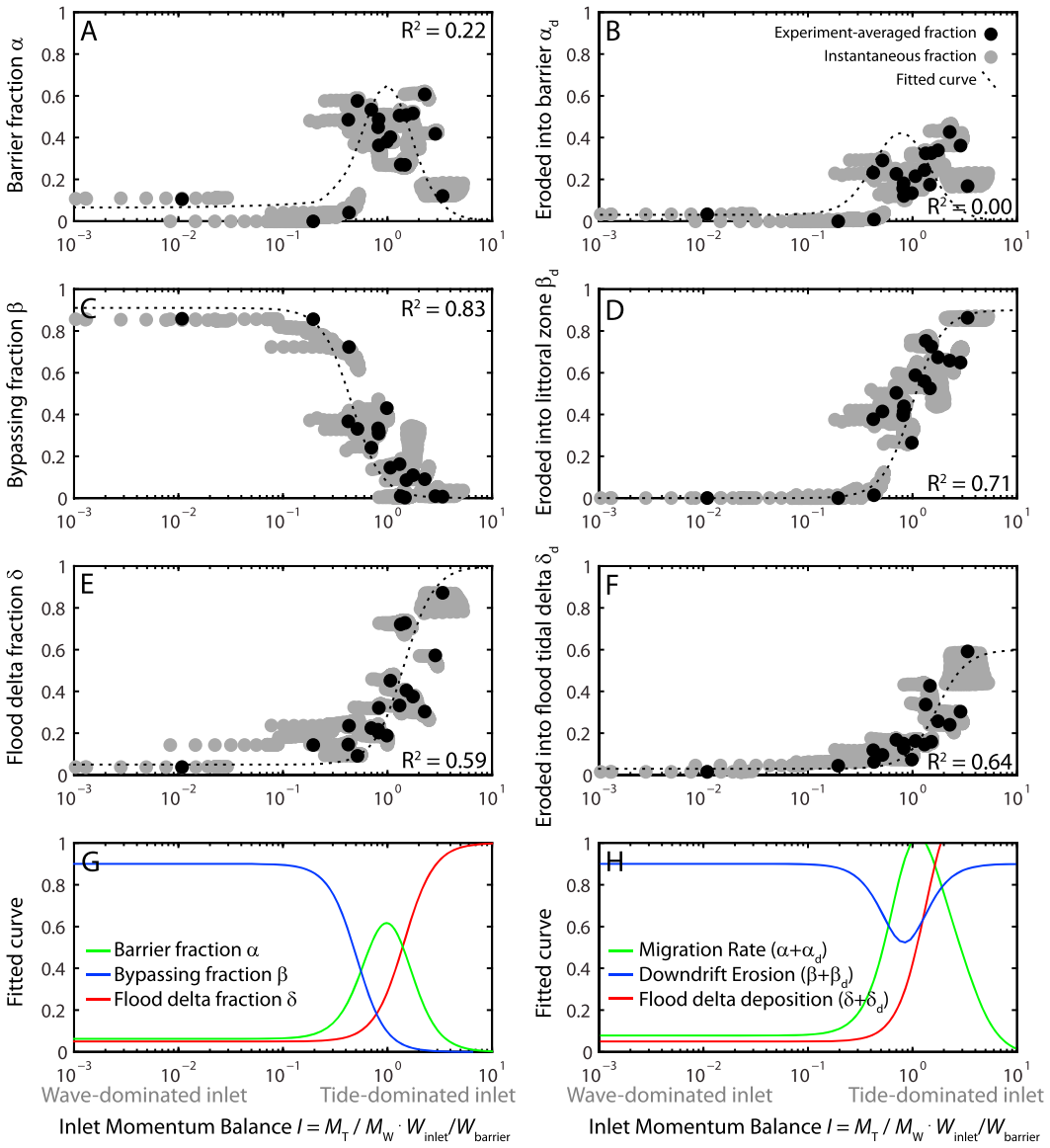

Figure 12. (a–f) Sediment distribution fractions α, β, δ, α_d, β_d, and δ_d plotted as a function of the tidal inlet momentum balance I (equation (5)). Black markers indicate the average of each model experiment; grey markers are cumulative values taken every 18 morphological minutes. Dotted lines show the fitted functions (equation (6)). (g) Fitted functions for α, β, and δ. (h) Aggregate deposition of new barrier growth (green), downdrift of the barrier (blue), and in the flood-tidal delta (red).

between the inlet width (W_{inlet}) and the barrier width (W_{barrier}) to define the nondimensional inlet momentum balance I:

$$I = \frac{M_T}{M_W} \cdot \frac{W_{\text{inlet}}}{W_{\text{barrier}}}. \tag{5}$$

Importantly, this quantity, which balances flood-tidal delta deposition with alongshore sediment bypassing, can be established a priori (without observing inlet migration). This allows for prediction of inlet sediment partitioning and tidal inlet migration based on quantities that can be measured in both our model experiments and in the field.

As expected, we find that alongshore sediment bypassing β is large for wave-dominated inlets (small I) and minimal for tide-dominated inlets (large I) (Figure 12c). For tide-dominated inlets, the volume of

Table 1. Fitted Values *a*, *b*, *c* and *d* for Sediment Fractions β, β_d, δ, and δ_d ($\alpha = 1 - \beta - \delta$ and $\alpha_d = \frac{3}{5}\alpha$) (Equation (6))

	a	*b*	*c*	*d*
β	0	0.9	10	3
β_d	0	0.9	0.9	−3
δ	0.05	0.95	3	−3
δ_d	0.03	0.57	3	−3

sediment eroded from the downdrift inlet bank is of similar order of magnitude as the littoral transport ($\alpha_d + \beta_d + \delta_d = O(1)$). Also, flood-tidal delta deposition is extensive for tide-dominated inlets (Figure 12e).

Tidal inlets that are "in balance" ($I \sim 1$) such that neither bypassing nor alongshore sediment bypassing is large ("mixed-energy" tidal inlets) [see *Hayes*, 1979] show the fastest migration rates (Figure 12). For this intermediate case, the tidal-momentum flux is large enough to prevent bypassing and allow for erosion of the downdrift inlet flank but low enough to reduce flood-tidal delta expansion. The wave-momentum flux is large enough to allow for sediment deposition on the updrift inlet flank.

10. Application to Natural Examples

10.1. Predicting Sediment Flux Partitioning

To extend the findings from the Delft3D model experiments to natural examples, we fit functions to the trends we observe between tidal inlet momentum balance *I* and the sediment fractions α, β, δ, α_d, β_d, and δ_d (Figure 12). We choose a smooth sigmoid shape, in part because, as our model experiments do not cover the entire range of *I*, a sigmoid shape ensures convergence to constant values for the limits $I \to 1/\infty$ and $I \to \infty$. For β, β_d, δ, and δ_d, we choose the function $f(I)$:

$$f(I) = a + \frac{b}{1 + c \cdot I^d}, \tag{6}$$

where the constants *a*, *b*, *c*, and *d* are fitted through trial and error to visually match the trends within the observed fractions from the model experiments (Table 1) while enforcing conservation of mass, $\alpha = 1 - \beta - \delta$. Such an approach allows us to capture the "flavor" of the distinct trends in Figure 12 across many orders of magnitude for the value of *I* while acknowledging the spread of model results and allowing that the model experiments are not direct reproduction of natural inlets. For α_d, we fit the function $\alpha_d = \frac{3}{5}\alpha$ (Figure 11). These empirical fitted functions allow us to make first-order predictions of sediment partitioning for natural tidal inlets given a tidal inlet momentum balance *I* (equation (5)).

10.2. Applying Sediment Flux Partitioning Predictions

For an estimated tidal inlet momentum balance *I* and the empirical functions of sediment distribution around tidal inlets (Figures 12g and 12h), we can attempt to predict the migration rate of natural tidal inlets. For 57 inlets along the U.S. coastline, we retrieved hindcasted ocean wave data from WaveWatch III [*Chawla et al.,* 2013] and tidal inlet statistics from the U.S. Army Corps of Engineers Coastal Inlets Research Program database [*Carr and Kraus*, 2002]. We supplemented the inlet data set with additional inlets for which long-term migration rates were available, such as Chatham Inlet, MA [*Giese*, 1988], Katama Inlet, MA, (Figure 1) and New Inlet, NC [*Hasbrouck*, 2007]. See supporting information Table S3 for an overview of the natural tidal inlet estimated properties [*Komar*, 1971; *Everts et al.,* 1974; *DeAlteris et al.,* 1976; *Mason*, 1981; *Aubrey and Speer*, 1984; *Inman and Dolan*, 1989; *Stone et al.,* 1992; *Kennish*, 2001; *Cleary and FitzGerald*, 2003; *State of Florida*, 2009; *Stive et al.,* 2010; *Mallinson et al.,* 2010; *Nienhuis et al.,* 2015].

Most modern inlets along the U.S. coastline are actively maintained in place (dredging, engineered banks), which makes the momentum balance a meaningless estimate of the migration rate. For maintained inlets, however, their barrier width and their wave and tidal environment can still provide insight in the potential natural range of inlet sediment distribution fractions α, β, δ, α_d, β_d, and δ_d. For the 22 inlets that appear to be minimally maintained, we used historical records and NASA Landsat imagery to obtain their migration rates.

Calculating the inlet momentum balance *I* and the best fit prediction for sediment partitioning (equation (6)), the freely migrating inlets are predicted to be widely distributed across environments of high flood-tidal

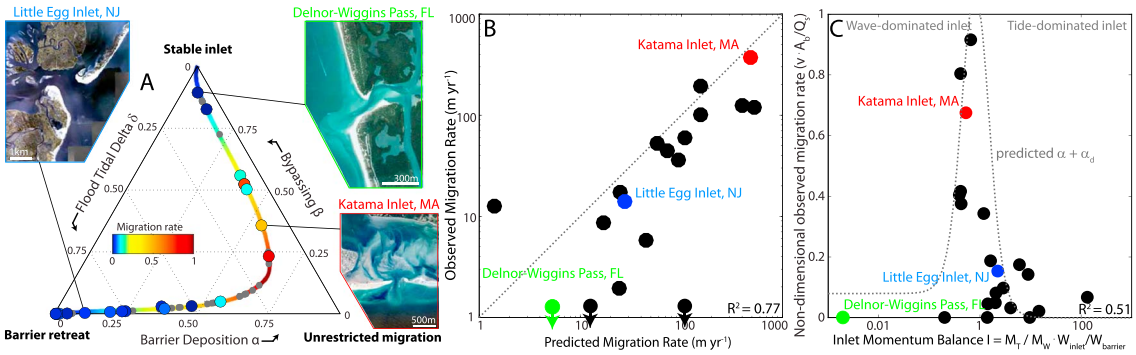

Figure 13. Analysis of natural tidal inlets along the U.S. coastline. (a) Predicted sediment distribution fractions for 57 tidal inlets (supporting information Table S3). For 22 inlets from which we could obtain migration rates, the color indicates the migration rate nondimensionalized by the littoral transport flux and the barrier cross-sectional area. (b) Predicted migration rate versus the observed migration rate for 22 natural inlets. Arrows indicate the inlet was not migrating (0 m yr^{-1}). (c) The nondimensional migration rate of the natural inlets ($v \times A_b/Q_s = \alpha + \alpha_d$) as a function of the calculated inlet momentum balance. The dotted line shows the independent prediction based on the Delft3D experiments.

delta deposition, inlet migration, and inlet bypassing defined using our ternary diagram (Figure 13a). Additionally, using our model-derived estimates of the fractions α, and α_d (section 10.1), we can attempt to predict inlet migration rates using equation (1). Comparing those predictions to the observed migration rate of 22 natural inlets, we find a surprisingly good agreement (Figure 13b and see also Table S3).

From the observed migration rates of the 22 natural inlets we can obtain estimates of the normalized migration rates ($\alpha + \alpha_d$, equation (1)). The natural examples show a peak in the normalized migration rate for an intermediate value of I—migration for these samples is indeed highest when the wave-momentum flux and the tide-momentum flux are of comparable magnitude (Figure 13c). Below, we highlight three examples.

First, at Little Egg Inlet, NJ, where $I = 2.3$, we predict that the majority of littoral sediment and eroded bank sediment should contribute to flood-tidal delta deposition. In this tidally dominated inlet (Figure 13) littoral sediment is not able to bypass ($\beta = 0.01$), and a relatively low fraction of the littoral sediment contributes to inlet migration ($\alpha = 0.19$). Our prediction of low β is supported by the observed drumstick morphology of the Little Egg Inlet and the adjacent barrier coast, a geometry suggestive of low alongshore sediment bypassing [*Fitzgerald*, 1988]. Between 1843 and 1934, the Little Egg Inlet has experienced an average migration rate of about 14 m yr^{-1} [*DeAlteris et al.,* 1976], close to our prediction of 27 m yr^{-1}.

Katama Inlet, MA, was a rapidly migrating inlet from its recent opening in 2007 before it closed in 2015, with observed migration rates of about 375 m yr^{-1} (Figures 1 and 13b) Our momentum flux ratio suggests that the wave-momentum flux and the tidal-momentum flux are in balance ($I = 0.5$), such that about 50% of the littoral sediment transport aids inlet migration. This leads to a predicted migration rate of 484 m yr^{-1}, relatively close to the observed average migration rate of about 375 m yr^{-1}. Bypassing is also predicted to be relatively high at $\beta = 0.4$, whereas only about 10% of the littoral sediment ends up in the flood-tidal delta. Using the linear relationship between α and α_d (Figure 11), we estimate that 40% of the newly formed barrier island is composed of eroded barrier island.

Because the alongshore component of the wave-momentum flux is significantly larger than the tidal-momentum flux, Delnor-Wiggins Pass, FL, is estimated to bypass most of the littoral sediment around the inlet ($\beta = 0.9$, $I = 3.4 \times 10^{-3}$) and to have a constricted channel that tends to closure. Although we are not aware of any detailed studies, the Florida state management plan documents frequent natural closures before maintenance dredging began in 1952 [*State of Florida*, 2009]. We predict a low migration rate (~5 m yr^{-1}) and do not observe any significant migration over the last decades (Figure 11b).

11. Discussion

In this study, we modeled wave-driven tidal inlet migration in Delft3D-SWAN. Our model experiments allowed us to investigate tidal inlet migration mechanisms and enabled us to formulate quantitative relations between the inlet environment and sources and sinks of sediment that contribute to inlet migration. Model

experiments suggest that alongshore sediment bypassing and flood-tidal delta deposition are important processes that affect not only the migration rate of tidal inlets but also the resulting morphology of the barrier coast (Figure 10). Inlets dominated by waves tend to bypass sediment and therefore migrate slowly; when inlet momentum fluxes are dominant, sediment accumulates in the flood-tidal delta. Between these end-members, when the wave-momentum flux and the tide-momentum flux are in balance, tidal inlets migrate rapidly as both alongshore sediment bypassing and flood-tidal delta deposition are limited (Figure 12). By migrating rapidly, there is new accommodation space in the tidal basin for flood-tidal delta deposits such that inlets become an efficient sink of littoral sediment.

11.1. Short-Term and Long-Term Fluctuations

In our model experiments and our mass balance framework of inlet migration, we assume that yearly to decadal timescale morphodynamics control tidal inlet steady state behavior. Many tidal inlets, however, show significant variation caused by episodic storms, tidal variability, and seasonal wave climate changes. Individual storms account for a large fraction of sediment overwashing barrier islands [*Donnelly et al.,* 2006], and some inlets have been observed to close seasonally [*Ranasinghe and Pattiaratchi*, 2003]. On yearly timescales, the volume of the ebb-tidal delta can vary substantially due to intermittent alongshore sediment bypassing [*Fitzgerald*, 1982], changes in wave climate, or changes in the tidal basin [*de Vriend et al.,* 1994]. Even though many short-term fluctuations in wave and tidal conditions occur, observed tidal inlet channel migration is often remarkably steady on decadal timescales [e.g., *Giese*, 1988; *Inman and Dolan*, 1989; *Hasbrouck*, 2007], perhaps owing to the persistence of littoral sediment transport. Waves in our model experiments all approach from 40°, future studies could address the (seasonal) effects of wave climate changes and ebb-tidal delta changes on inlet migration. Additionally, future studies could take into account the wind-driven aggradation of dunes atop the newly formed barrier, which can represent a significant part of the updrift sediment budget [*Kumar and Sanders*, 1974].

11.2. Implications for Barrier Island Evolution

In migrating tidal inlets, flood-tidal deltas can grow at rates greater than the littoral sediment flux (up to 1.5 times) by accumulating sediment from both the updrift littoral sediment source and the downdrift eroded barrier sediment (Figure 12h). By leaving a zone of flood-tidal delta deposits in its wake, a migrating inlet is an efficacious sediment transport sink that can contribute to the landward migration of barrier islands.

The potential of migrating inlets to transgress barrier systems may have significant implications for barrier system response to sea level rise. The fate of modern barrier islands on coasts with rapid and accelerating sea level rise depends greatly on the retreat rate barrier islands can achieve. Many models of barrier island response to sea level rise consider landward retreat to depend on overwash fluxes: storm-induced episodic sediment supplied from the nearshore environment that overtops barriers and is deposited on backbarrier marshes [*Stolper et al.,* 2005; *Lorenzo-Trueba and Ashton*, 2014]. Given that 50% of barrier complexes show tidal inlet fill sequences [*Moslow and Tye*, 1985], inlet migration, through flood-tidal delta deposition, is likely also an important sediment mover that allows barrier islands to transgress.

Storm overwash and tidal inlet formation are closely coupled. The location of inlet formation is dependent on the potential tidal prism combined with local barrier island topography during storms [*Leatherman*, 1979], although sometimes the formation of tidal inlets is dictated by the underlying geology in the form of abandoned fluvial channels [*van Veen*, 1950]. In many locations, overtopping overwash can be viewed as storm deposits where the tidal flow potential was insufficient to generate a permanent tidal inlet [*Pierce*, 1970].

The magnitude of storm overwash is dependent on barrier island and lagoonal topography [*Donnelly et al.,* 2006]. Here we also find a dependence on backbarrier bathymetry and barrier geometry for tidal inlets: flood-tidal delta volumes are low for shallow basins (Figure 8) and wide barriers (Figure 9). On long timescales, the net import of littoral sediment for a particular stretch of barrier coast will therefore decrease for each passing inlet if there was no increase in lagoonal accommodation space by either sea level rise or subsidence. Additionally, barrier widening by flood-tidal delta welding can decrease the likelihood of inlet formation and increase the likelihood of inlet closure. We conjecture that the decreasing effectiveness of inlets as a sediment sink for increasing barrier width or decreasing basin depth could be viewed analogously to the critical barrier width concept for storm overwash [e.g., *Leatherman*, 1979], such that through repeated

migration, a stretch of barrier coast dominated by tidal inlets may attain sufficient width that migration slows and flood tidal deltas cease to grow. At this point the inlet no longer acts as an onshore sediment sink. Such a conjectured limiting width is not necessarily the same as a storm overwash dominated barrier width: for the North Carolina Outer Banks, barrier islands composed of inlet-fill sequences tend to be wider than barrier islands composed of storm overwash sediments [*Mallinson et al.,* 2010].

12. Conclusions

In this study, we have investigated tidal inlet morphodynamics and migration using model experiments in Delft3D-SWAN. Modeled inlets migrate because of asymmetry in sediment transport processes between the updrift and downdrift flanks of the inlet: wave breaking and tidal currents erode sediment into the basin primarily along the downdrift bank. As an inlet migrates, previously deposited flood-tidal delta in the backbarrier of the newly formed barrier island restricts flow and promotes sediment deposition along the updrift bank, which further increases inlet migration by forcing flow around the downdrift flank.

To quantify tidal inlet migration for both model experiments and natural examples, we present a mass balance model of inlet migration that incorporates multiple sediment pathways, including littoral sediment bypassing and the fate of sediment eroded from the downdrift inlet bank. Delft3D model experiments show that tidal inlet migration is maximized when the wave- and tidal-momentum flux are in balance when scaled in proportion to the inlet width to barrier width ratio, resulting in reduced alongshore sediment bypassing and flood-tidal delta deposition. For rapidly migrating tidal inlets that continue to expose new tidal basin for flood-tidal delta deposition, inlets can act as a significant sediment sink on the order of the littoral sediment flux itself. By parameterizing our model experiments, we have provided predictions of migration rates for natural inlets, showing good agreement with observed migration rates of 22 inlets along the U.S. East Coast.

Acknowledgments

This research was supported by National Science Foundation grant EAR-1424728. We thank Julie Rosati for help with the U.S. Army Corps of Engineers' Coastal Inlets Research Program Federal Inlets database, and we also thank Tim Nelson, Jeff List, and Maarten van Ormondt for fruitful discussions on tidal inlet modeling. We acknowledge the helpful comments from the Editor Giovanni Coco, the Associate Editor Ton Hoitink, and Ian Townend and two anonymous reviewers. The data used are listed in the supporting information. Unprocessed model outputs are available upon request from the authors.

References

Airy, G. B. (1841), Tides and waves, *Encycl. Metrop.*, *3*, 396.

Ashton, A. D., J. H. Nienhuis, and K. Ells (2016), On a neck, on a spit: Controls on the shape of free spits, *Earth Surf. Dyn.*, *4*(1), 193–210, doi:10.5194/esurf-4-193-2016.

Aubrey, D. G., and P. E. Speer (1984), Updrift migration of tidal inlets, *J. Geol.*, *92*(5), 531–545.

Booij, N., R. C. Ris, and L. H. Holthuijsen (1999), A third-generation wave model for coastal regions: 1. Model description and validation, *J. Geophys. Res.*, *104*, 7649–7666, doi:10.1029/98JC02622.

Bruun, P. (1978), in *Stability of Tidal Inlets: Theory and Engineering*, edited by A. J. Mehta and I. G. Johnsson, Elsevier Sci., Amsterdam.

Bruun, P., and F. Gerritsen (1959), Natural by-passing of sand at coastal inlets, *J. Waterw. Harbors Div.*, *85*(4), 75–107.

Carr, E. E., and N. C. Kraus (2002), Federal inlets database, Vicksburg, Miss.

Chawla, A., D. M. Spindler, and H. L. Tolman (2013), Validation of a thirty year wave hindcast using the Climate Forecast System Reanalysis winds, *Ocean Modell.*, *70*, 189–206, doi:10.1016/j.ocemod.2012.07.005.

Cleary, W. J., and D. M. FitzGerald (2003), Tidal inlet response to natural sedimentation processes and dredging-induced tidal prism changes: Mason Inlet, North Carolina, *J. Coastal Res.*, *19*(4), 1018–1025.

Dastgheib, A. (2012), Long-term process-based morphological modeling of large tidal basins, Thesis, Delft Univ. of Technol.-UNESCO-IHE.

DeAlteris, J., T. McKinney, and J. Roney (1976), Beach Haven and Little Egg Inlet, A case study, *Coastal Eng.*, *15*, 1881–1898, doi:10.9753/icce.v15.%25p.

Dean, R. G. (1991), Equilibrium beach profiles: Characteristics and applications, *J. Coastal Res.*, *7*(1), 53–84.

Deltares (2014), *User Manual Delft 3D*, Deltares, Delft, The Netherlands.

de Swart, H. E., and J. T. F. Zimmerman (2009), Morphodynamics of tidal inlet systems, *Annu. Rev. Fluid Mech.*, *41*, 203–229, doi:10.1146/annurev.fluid.010908.165159.

de Vriend, H. J., W. T. Bakker, and D. P. Bilse (1994), A morphological behaviour model for the outer delta of mixed-energy tidal inlets, *Coastal Eng.*, *23*(3–4), 305–327, doi:10.1016/0378-3839(94)90008-6.

Dodet, G. (2013), Morphodynamic modelling of a wave-dominated tidal inlet: The Albufeira lagoon, Thesis, Univ. de La Rochelle.

Donnelly, C., N. Kraus, and M. Larson (2006), State of knowledge on measurement and modeling of coastal overwash, *J. Coastal Res.*, *22*(4), 965–991, doi:10.2112/04-0431.1.

Escoffier, F. F. (1940), The stability of tidal inlets, *Shore Beach*, *8*(4), 114–115.

Everts, C. H., A. E. Dewall, and M. T. Czemiak (1974), Behavior of beach fill at Atlantic City, New Jersey, in *Coastal Engineering 1974*, pp. 1370–1388, Am. Soc. of Civil Eng., Copenhagen.

Fenster, M., and R. Dolan (1996), Assessing the impact of tidal inlets on adjacent barrier island shorelines, *J. Coastal Res.*, *12*(1), 294–310.

Fitzgerald, D. M. (1982), Sediment bypassing at mixed energy tidal inlets, in *Proceedings of 18th Conference of Coastal Engineering*, vol. 18, edited by B. L. Edge, pp. 1094–1118, ASCE, Cape Town, South Africa.

Fitzgerald, D. M. (1988), Shoreline erosional-depositional processes associated with tidal inlets, in *Lecture Notes on Coastal and Estuarine Studies*, vol. 29, edited by D. G. Aubrey and L. Weishar, pp. 186–225, Springer, New York.

Giese, G. S. (1988), Cyclical behavior of the tidal inlet at Nauset Beach, Chatham, Massachusetts, in *Lecture Notes on Coastal Estuarine Studies*, vol. 29, edited by D. G. Aubrey and L. Weishar, pp. 269–283, Springer, New York.
Hasbrouck, E. G. (2007), The influence of tidal inlet migration and closure on barrier planform changes: Federal Beach, NC, Thesis, Univ. of North Carolina, Wilmington.
Hayes, M. O. (1979), Barrier island morphology as a function of tidal and wave regime, in *Barrier Islands*, edited by S. P. Leatherman, pp. 1–27, Academic Press, New York.
Hayes, M. O. (1980), General morphology and sediment patterns in tidal inlets, *Sediment. Geol.*, *26*(1–3), 139–156, doi:10.1016/0037-0738(80)90009-3.
Hine, A. C. (1975), Bedform distribution and migration patterns on tidal deltas in the Chatham Harbor Estuary, Cape Cod, Massachusetts, in *Estuarine Research*, vol. 2, edited by L. E. Cronin, pp. 235–252, Academia, New York.
Hoan, L. X., H. Hanson, M. Larson, and S. Kato (2011), A mathematical model of spit growth and barrier elongation: Application to Fire Island Inlet (USA) and Badreveln Spit (Sweden), *Estuarine Coastal Shelf Sci.*, *93*(4), 468–477, doi:10.1016/j.ecss.2011.05.033.
Hubbard, D. K., G. Oertel, and D. Nummedal (1979), The role of waves and tidal currents in the development of tidal-inlet sedimentary structures and sand body geometry: Examples from North Carolina, South Carolina, and Georgia, *J. Sediment. Petrol.*, *49*(4), 1073–1091.
Inman, D. L., and R. Dolan (1989), The Outer Banks of North Carolina: Budget of sediment and inlet dynamics along a migrating barrier system, *J. Coastal Res.*, *5*(2), 193–237.
Johnson, D. W. (1919), *Shore Processes and Shoreline Development*, 1st ed., John Wiley, New York.
Kennish, M. J. (2001), Physical description of the Barnegat Bay—Little Egg Harbor Estuarine System, *J. Coastal Res.*, *32*(SI), 13–27.
Komar, P. D. (1971), Mechanics of sand transport on beaches, *J. Geophys. Res.*, *76*, 713–721, doi:10.1029/Jc076i003p00713.
Komar, P. D. (1996), Tidal-inlet processes and morphology related to the transport of sediments, *J. Coastal Res.*, *23*(SI), 23–45.
Kraus, N. C. (1999), Analytical model of spit evolution at inlets, in *Coastal Sediments '99*, edited by N. C. Kraus and W. G. McDougal, pp. 1739–1754, ASCE, New York.
Kraus, N. C. (2000), Reservoir model of ebb-tidal shoal evolution and sand bypassing, *J. Waterw. Port Coastal Ocean Eng.*, *126*, 305–313, doi:10.1061/(ASCE)0733-950X(2000)126:6(305).
Kraus, N. C. (2002), Reservoir model for calculating natural sand bypassing and change in volume of ebb-tidal shoals: Description, Vicksburg, Miss.
Kumar, N., and J. E. Sanders (1974), Inlet sequence: A vertical succession of sedimentary structures and textures created by the lateral migration of tidal inlets, *Sedimentology*, *21*(4), 491–532, doi:10.1111/j.1365-3091.1974.tb01788.x.
Leatherman, S. P. (1979), Migration of Assateague Island, Maryland, by inlet and overwash processes, *Geology*, *7*(2), 104–107, doi:10.1130/0091-7613(1979)7<104:MOAIMB>2.0.CO;2.
List, J. H., and A. D. Ashton (2007), A circulation modeling approach for evaluating the conditions for shoreline instabilities, in *Coastal Sediments '07*, edited by N. C. Kraus and J. D. Rosati, pp. 1–14, Am. Soc. of Civil Eng., New Orleans, La.
Lorenzo-Trueba, J., and A. D. Ashton (2014), Rollover, drowning, and discontinuous retreat: Distinct modes of barrier response to sea-level rise arising from a simple morphodynamic model, *J. Geophys. Res. Earth Surf.*, *119*, 779–801, doi:10.1002/2013JF002941.
Mallinson, D. J., C. W. Smith, S. J. Culver, S. R. Riggs, and D. Ames (2010), Geological characteristics and spatial distribution of paleo-inlet channels beneath the outer banks barrier islands, North Carolina, USA, *Estuarine Coastal Shelf Sci.*, *88*(2), 175–189, doi:10.1016/j.ecss.2010.03.024.
Mason, C. (1981), *Hydraulics and Stability of Five Texas Inlets*, Fort Belvoir, Coastal Engineering Research Center, Virginia.
McGee, W. J. (1890), *Encroachments of the Sea*, Forum Co., New York.
Moslow, T. F., and S. D. Heron (1978), Relict inlets: Preservation and occurrence in the Holocene Stratigraphy of Southern Core Banks, North Carolina, *J. Sediment. Res.*, *48*(4), 1275–1286.
Moslow, T. F., and R. S. Tye (1985), Recognition and characterization of Holocene tidal inlet sequences, *Mar. Geol.*, *63*(1–4), 129–151, doi:10.1016/0025-3227(85)90081-7.
Murray, A. B. (2007), Reducing model complexity for explanation and prediction, *Geomorphology*, *90*(3–4), 178–191, doi:10.1016/j.geomorph.2006.10.020.
Nahon, A., X. Bertin, A. B. Fortunato, and A. Oliveira (2012), Process-based 2DH morphodynamic modeling of tidal inlets: A comparison with empirical classifications and theories, *Mar. Geol.*, *291–294*, 1–11, doi:10.1016/j.margeo.2011.10.001.
Nienhuis, J. H., A. D. Ashton, and L. Giosan (2015), What makes a delta wave-dominated? *Geology*, *43*(6), 511–514, doi:10.1130/G36518.1.
Nienhuis, J. H., A. D. Ashton, W. Nardin, S. Fagherazzi, and L. Giosan (2016), Alongshore sediment bypassing as a control on river mouth morphodynamics, *J. Geophys. Res. Earth Surf.*, *121*, 664–683, doi:10.1002/2015JF003780.
O'Brien, M. P. (1966), Equilibrium flow areas of tidal inlets on sandy coasts, in *Coastal Engineering*, edited by J. W. Johnson, pp. 676–686, ASCE, Tokyo.
Oertel, G. F. (1977), Geomorphic cycles in ebb deltas and related patterns of shore erosion and accretion, *J. Sediment. Res.*, *47*(3), 1121–1131, doi:10.1306/212F72F2-2B24-11D7-8648000102C1865D.
Pierce, J. W. (1970), Tidal inlets and washover fans, *J. Geol.*, *78*(2), 230–234.
Powell, M. A., R. J. Thieke, and A. J. Mehta (2006), Morphodynamic relationships for ebb and flood delta volumes at Florida's tidal entrances, *Ocean Dyn.*, *56*(3–4), 295–307, doi:10.1007/s10236-006-0064-3.
Ranasinghe, R., and C. Pattiaratchi (2003), The seasonal closure of tidal inlets: Causes and effects, *Coastal Eng. J.*, *45*(4), 601–627, doi:10.1142/S0578563403000919.
Ridderinkhof, W., H. E. de Swart, M. van der Vegt, N. C. Alebregtse, and P. Hoekstra (2014), Geometry of tidal inlet systems: A key factor for the net sediment transport in tidal inlets, *J. Geophys. Res. Oceans*, *119*, 6988–7006, doi:10.1002/2014JC010226.
Roos, P. C., H. M. Schuttelaars, and R. L. Brouwer (2013), Observations of barrier island length explained using an exploratory morphodynamic model, *Geophys. Res. Lett.*, *40*, 4338–4343, doi:10.1002/grl.50843.
Sha, L. P., and J. H. van den Berg (1993), Variation in ebb-tidal delta geometry along the Coast of the Netherlands and the German Bight, *J. Coastal Res.*, *9*(3), 730–746, doi:10.2307/4298126.
State of Florida (2009), Delnor-Wiggins Pass State Park Unit Management Plan, Tallahassee, Fla.
Stive, M. J. F., L. Ji, R. L. Brouwer, J. C. van de Kreeke, and R. Ranasinghe (2010), Empirical relationship between inlet cross-sectional area and tidal prism: A re-evaluation, in *Proceedings of the 32nd International Conference in Coastal Engineering*, edited by J. McKee Smith and P. Lynett, pp. 1–10, Coastal Eng. Res. Counc., Shanghai, China.
Stolper, D., J. H. List, and E. R. Thieler (2005), Simulating the evolution of coastal morphology and stratigraphy with a new morphological-behaviour model (GEOMBEST), *Mar. Geol.*, *218*(1–4), 17–36, doi:10.1016/j.margeo.2005.02.019.
Stommel, H., and H. G. Former (1952), *On the Nature of Estuarine Circulation*, Woods Hole Oceanogr. Inst., Woods Hole, Mass.

Stone, G. W., F. W. Stapor, J. P. May, J. P. Morgan, F. W. Stapor Jr., J. P. May, and J. P. Morgan (1992), Multiple sediment sources and a cellular, non-integrated, longshore drift system: Northwest Florida and southeast Alabama coast, USA, *Mar. Geol.*, *105*(1–4), 141–154, doi:10.1016/0025-3227(92)90186-L.

Tung, T. T., D. R. Walstra, J. van de Graaff, and M. J. F. Stive (2009), Morphological modeling of tidal inlet migration and closure, *J. Coastal Res.*, *IS56*, 1080–1084.

van der Vegt, M., H. M. Schuttelaars, and H. E. de Swart (2006), Modeling the equilibrium of tide-dominated ebb-tidal deltas, *J. Geophys. Res.*, *111*, F02013, doi:10.1029/2005JF000312.

van Rijn, L. C. (1993), *Principles of Sediment Transport in Rivers, Estuaries and Coastal Seas*, 1st ed., Aqua Publ., Amsterdam.

van Veen, J. (1950), Eb- en Vloedschaar Systemen in de Nederlandse Getijwateren, Tijdschrift Koninklijk Nederlansch Aardrijkskundig Genootschap, vol. 67, pp. 303–325.

Walton, T. L. Jr., and W. Adams (1977), Capacity of inlet outer bars to store sand, *Coastal Eng.* 1976, 1919–1937, doi:10.1061/9780872620834.112.